Supplement of Ocean Sci., 20, 1547–1566, 2024
https://doi.org/10.5194/os-20-1547-2024-supplement

Ocean Science Open Access EGU

Supplement of

Influence of river runoff and precipitation on the seasonal and interannual variability of sea surface salinity in the eastern North Tropical Atlantic

Clovis Thouvenin-Masson et al.

Correspondence to: Clovis Thouvenin-Masson (clovis.thouvenin-masson@locean.ipsl.fr) and Jacqueline Boutin (jb@locean.ipsl.fr)

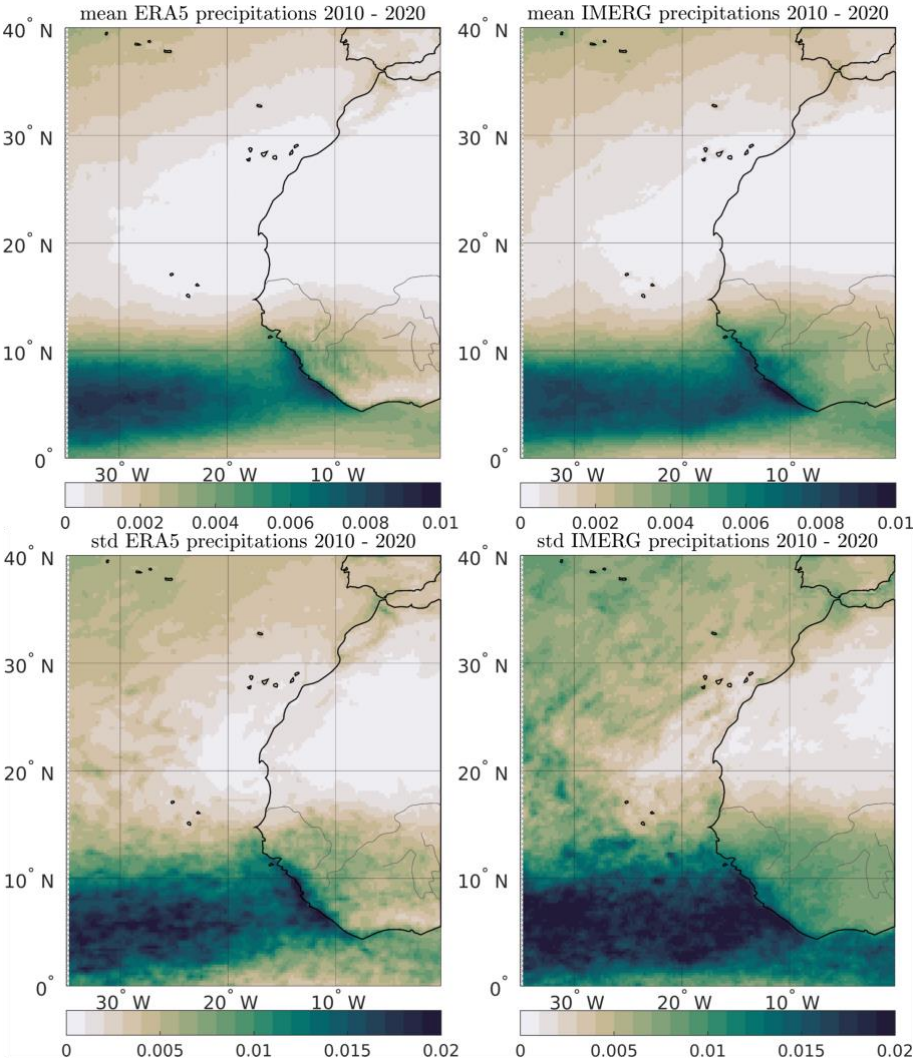

Figure S1: Distribution of ERA5 (left) and IMERG (right) precipitation (in m/day). Average precipitation between 2010 and 2019 (top), standard deviation of precipitation over the same period (bottom).

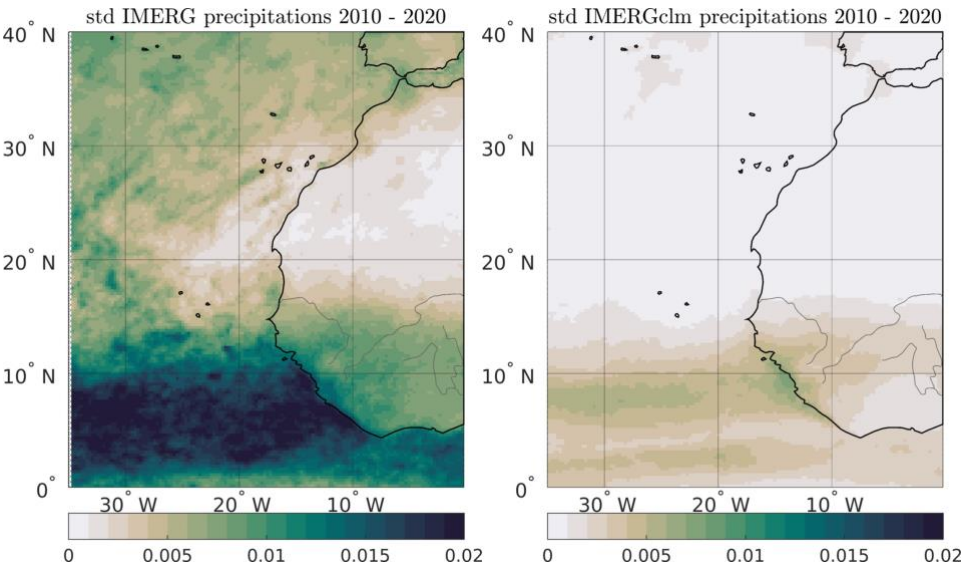

Figure S2: Standard deviation of IMERG precipitation (in m/day) (left) and the one used in the CROCOprclm simulation (right) over 2010-2020.

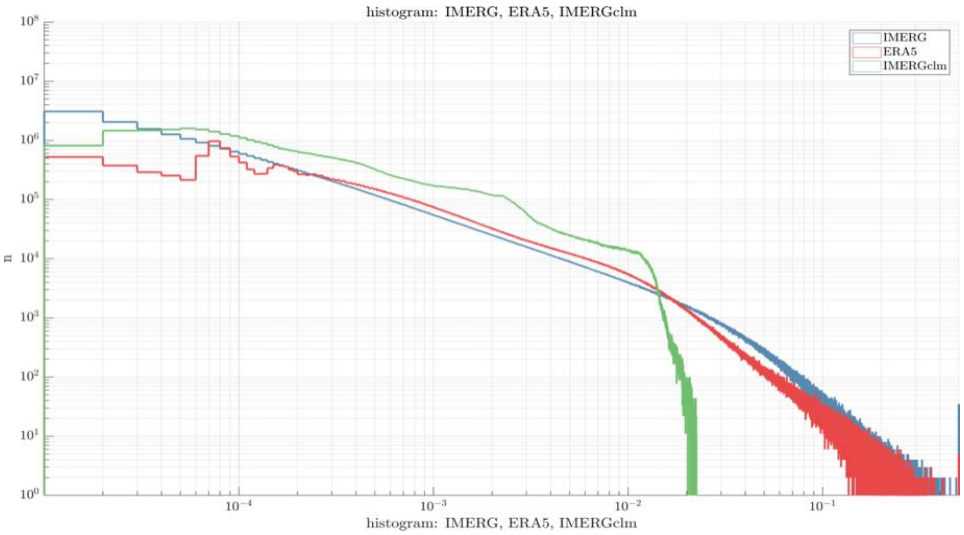

Figure S3: Histogram of the ERA5 precipitation (red), IMERG precipitation (blue) and monthly-mean climatological precipitation (in m/day) used in the CROCOprclm simulation (green). Note that scales are logarithmic.

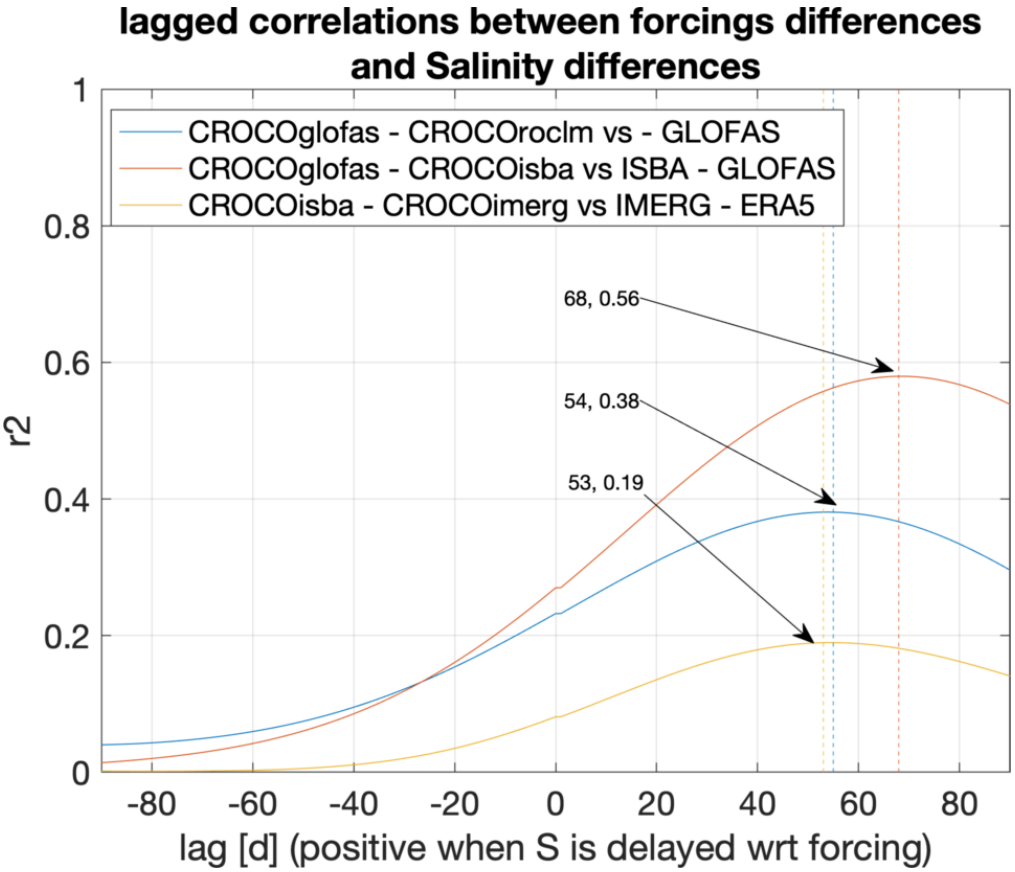

Figure S4: Correlations between the curves displayed in Figure 7, as a function of the applied time lag. Blue: Panel 7a; red: Panel 7b; yellow: Panel 7c. The lags chosen in the article correspond to the maximum correlation (indicated by an arrow for each of the curves).

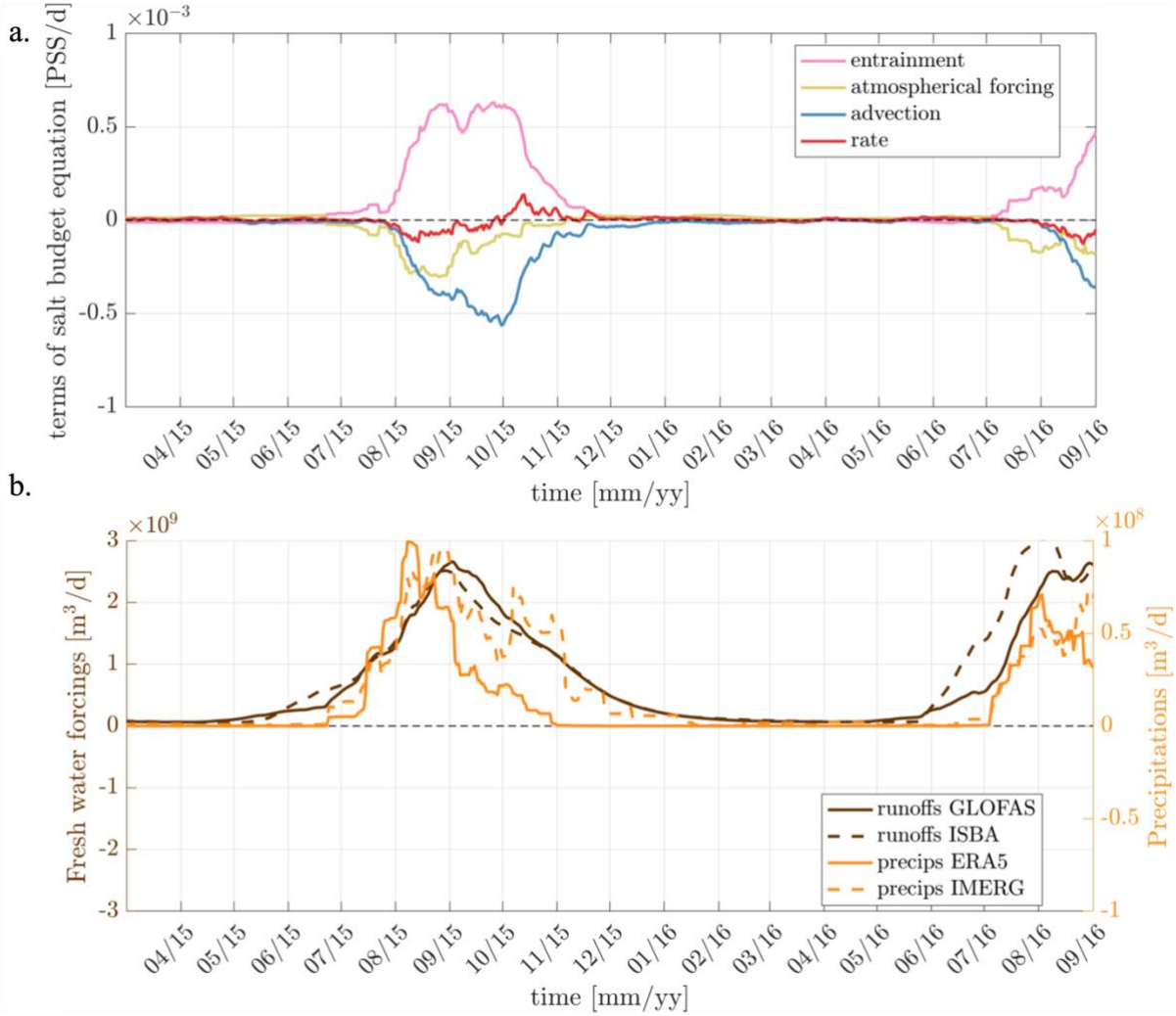

Figure S5: (a) Anomalies in the terms (in pss/day) of the salinity balance equation of the CROCOglofas simulation and (b) anomalies in the corresponding forcings at the Melax point. The colors in (a) are identical to those in Figure 2c. The colors in (b) are identical to those in Figure 2b.

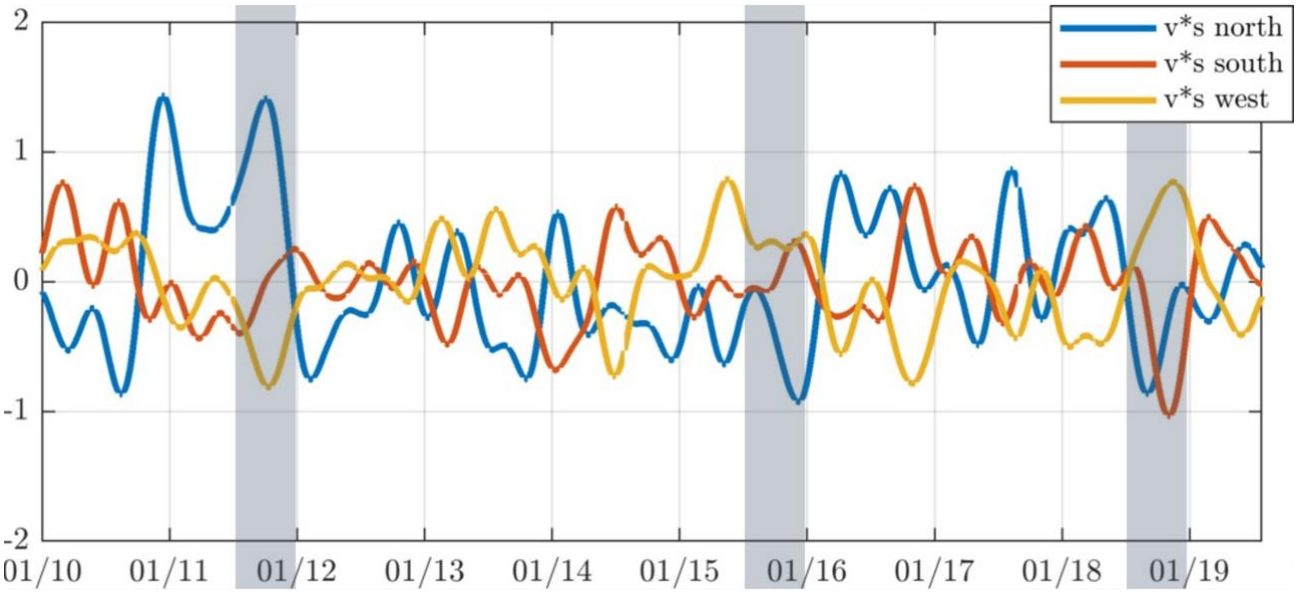

Figure S6: Band-pass filtered anomalies (using a three-month running mean) in anomalous salt flux (V'.<S>) through the boundaries of the e-NTA region due to a surface current anomaly (V') multiplied by climatological salinity <S> at the border. Blue line: flux through the northern boundary; red line: flux through the southern boundary; yellow line: flux through the western boundary. Positive flux indicates a salt input in the e-NTA region.

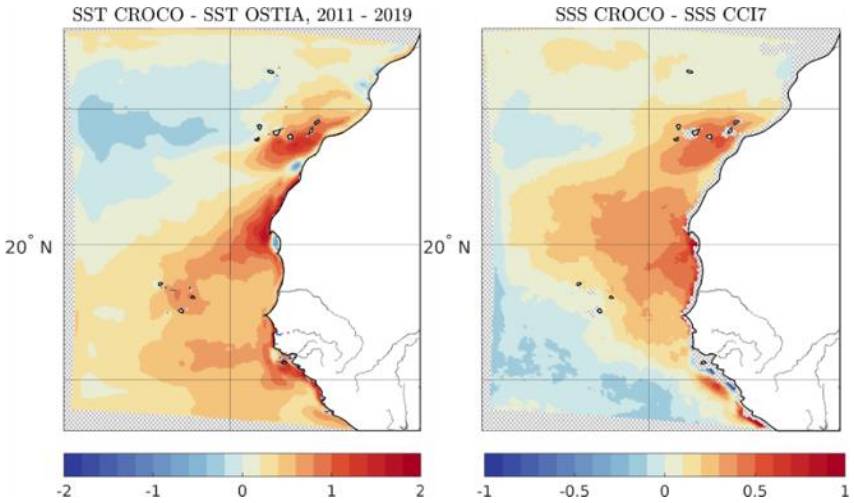

Figure S7: (left) Average SST bias (in °C) between CROCOglofas simulated SST and OSTIA SST and (right) average SSS bias (in pss) between the CROCOglofas simulated SSS and CCI SSS.

We observe a bias of the model in SST compared with the OSTIA (Operational Sea Surface Temperature and Ice Analysis; Donlon et al. (2012)) satellite SST (Figure a). Here we seek to determine whether this SST bias may be at the origin of the SSS bias discussed in the body of the article (Figure b). Indeed, a bias in SST generates an evaporation deviation, which has an influence on salinity in the mixed layer. The SSS bias resulting from the SST bias is estimated to first order using the bulk heat flux equations by the method described below: it is of the same order of magnitude as the SSS biases observed between CROCO and CCI (Figure).

Bulk formulations describe flows at the air-sea interface, including evaporation:

$$E = \rho C_q (q_0 - q_z) u$$

With E the evaporation, ρ the density, C_q the Bulk coefficient, u the wind speed at altitude z above the surface. q_z represents the specific humidity at altitude z, and q_0 the saturation specific humidity of the air at surface temperature θ_0;

q_z and q_0 are dependent on surface temperature and pressure, and are written as:

$$q_z = q_{sat}(d_z, SLP)$$

$$q_0 = 0.98 q_{sat}(\theta_0, SLP)$$

Noting SLP as the air pressure at the surface and e_{sat} as the partial pressure of water vapor, we can calculate the specific humidity at a temperature T from the following formula:

$$q_{\text{sat}}(T, SLP) = \frac{\epsilon e_{\text{sat}}(T)}{SLP - (1-\epsilon) e_{\text{sat}}(T)} \epsilon = 0.62$$

e_{sat} can be determined by the Goff Gratch equation:

$$\begin{gathered} log_{10}\left(e_{\text{sat}}(T)\right) = 10.79574(1 - T_0/T) \\ -5.028 log_{10}(T/T_0) \\ T_0 = 273.16 \\ +1.5047510^{-4}\left[1 - 10^{-82969(T/T_0 - 1)}\right] \\ +0.4287310^{-3}\left[10^{4.76955(1-T_0/T)} - 1\right] \\ +0.78614 \end{gathered}$$

Noting SSTi as the model SST and SSTf as the SST Ostia, switching from one to the other generates a difference in evaporation ΔE :

$$\frac{\Delta E}{E_i} = \frac{q_{0f} - q_{0i}}{q_{0i}} = \frac{q_{SAT}\left(T_f, SLP\right) - q_{SAT}(T_i, SLP)}{q_{SAT}(T_i, SLP)}$$

This difference is then incorporated into the salinity balance equation (equation 6), with the other terms (including mixed layer depth) unchanged at first order:

$$\Delta\, \partial_t \boldsymbol{S} = -\frac{\Delta E}{E_i} \,.\, E_i . \frac{S}{H}\Big|$$

This gives a change in the SSS rate at each time step, which can be added to the model's salinity trend. The mean deviation obtained is of the same order of magnitude as the deviation between CROCO SSS and CCI SSS, although generally smaller. The geographical pattern (not shown) is similar, although this is a rough estimate that does not take into account, for example, the advection of saltier waters obtained after this correction.

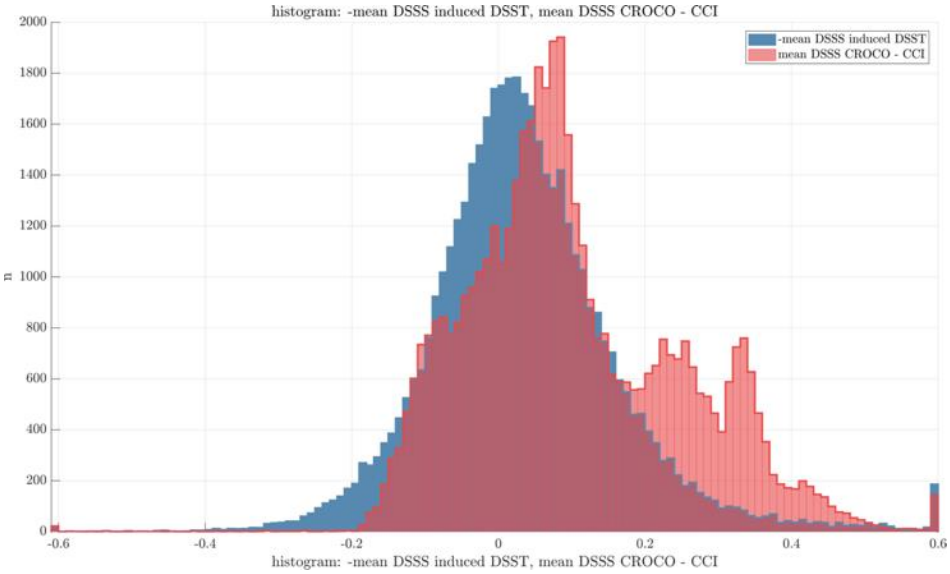

Figure S8: histogram showing the salinity bias between the CROCOglofas simulation and CCI (red) and the expected SSS bias linked to the SST bias (blue), in pss.

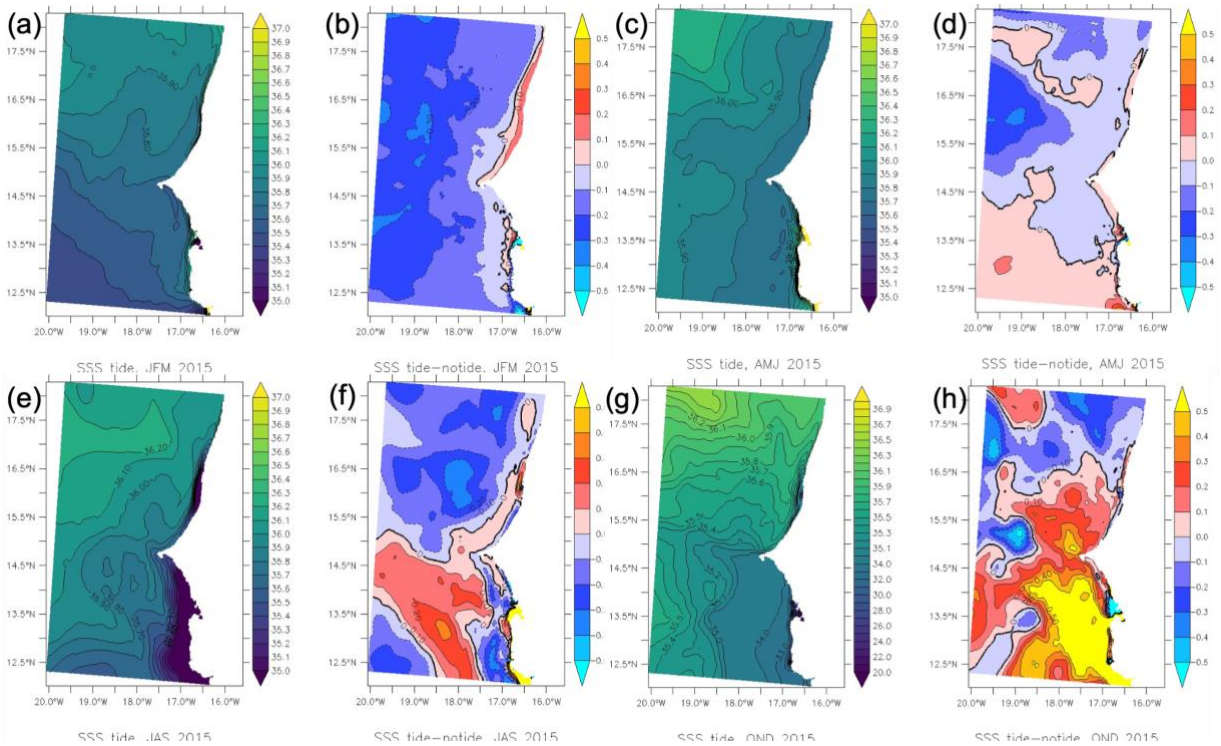

Figure S9: Effect of tides on Sea Surface Salinity (SSS), in pss, in the e-NTA region in 2015. The maps show the simulated salinity with tides (a, c, e, g) and the difference from simulations obtained without tides (b, d, f, h). Maps averaged over 3 months: JFM (January to March) (a, b), AMJ (April to June) (c, d), JAS (July to September) (e, f), OND (October to December) (g, h). The tidal effect on SSS, leading to an increase of SSS in the plume, is mostly seen in OND (h).

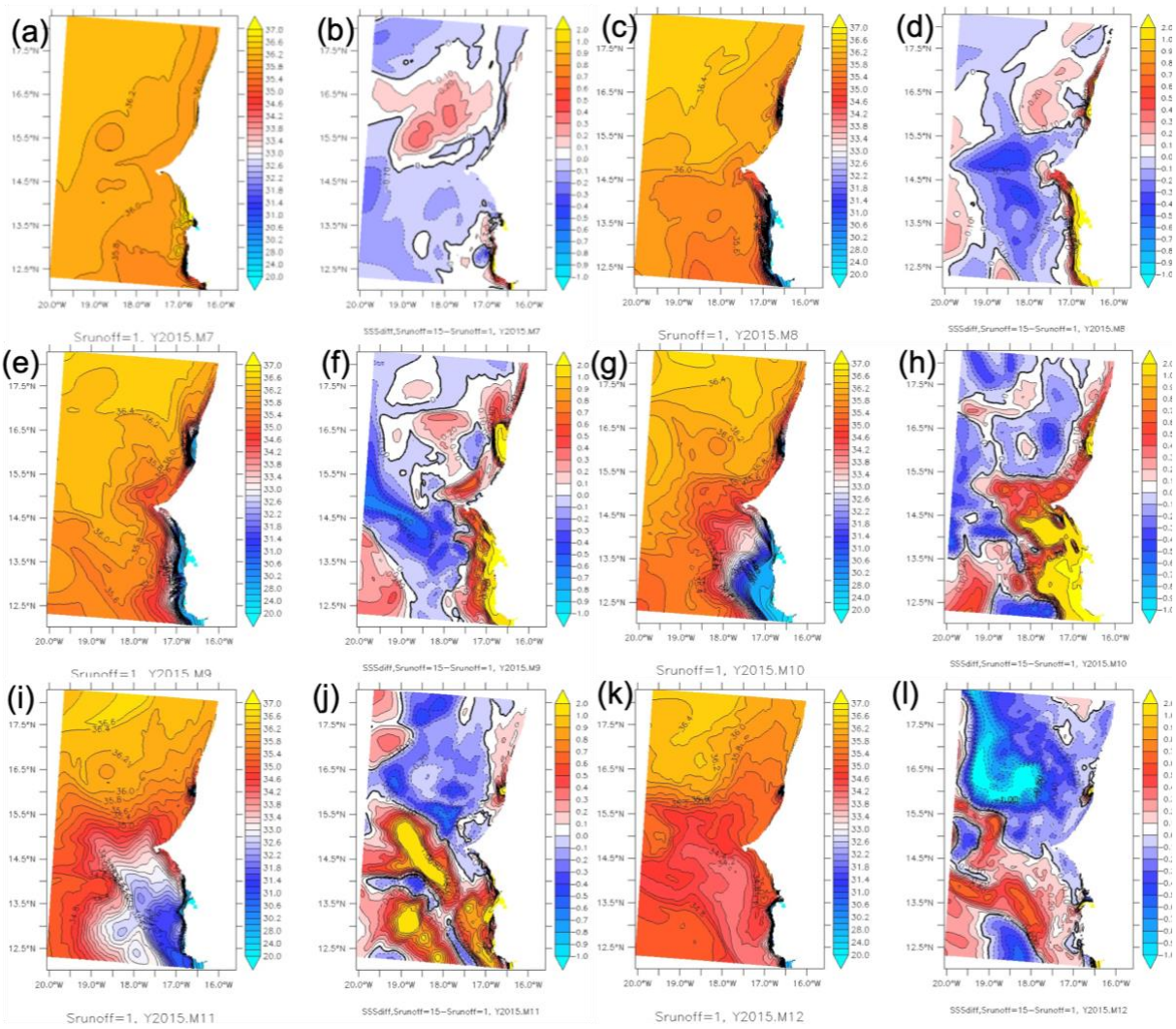

Figure S10: Effect of a change in river salinity on Sea Surface Salinity (SSS), in practical salinity units (psu), in the e-NTA region in 2015. The maps initially show the simulated salinity with river salinity of 1 pss (a, c, e, g, i, k) and the difference from simulations obtained with river salinity of 15 pss (b, d, f, h, j, l). Maps averaged over 1 month: July (a, b), August (c, d), September (e, f), October (g, h), November (i, j), December (k, l).